JOURNAL OF MATERIALS SCIENCE 25 (1990) 3753–3764

Effect of $ZrSiO_4$ and MgO additions on reaction sintering and properties of Al_2TiO_5–based materials

H. WOHLFROMM, J. S. MOYA, P. PENA
Instituto de Cerámica y Vidrio (C.S.I.C.), Arganda del Rey, Madrid, Spain

Two sets of Al_2TiO_5-based composites were prepared by reaction sintering of (a) $Al_2O_3/TiO_2/ZrSiO_4$ and (b) $Al_2O_3/TiO_2/ZrSiO_4/MgO$ powder mixtures. The influence of the variation of $ZrSiO_4$ content (0 to 10 wt%) and the addition of 2 wt% MgO on the reaction-sintering process, microstructure, mechanical and thermal properties, were evaluated. $ZrSiO_4$ addition shifted the Al_2TiO_5 formation to higher temperatures, whereas MgO accelerated both Al_2TiO_5 formation and $ZrSiO_4$ decomposition. The presence of $ZrSiO_4$ and an excess of Al_2O_3 generated a dispersion of ZrO_2 and mullite particles in the grain boundaries and enhanced simultaneously the densification process. After sintering in the temperature range 1350 to 1500° C, the obtained composites exhibited significantly higher bending strength than the monophasic aluminium titanate (up to 80 MPa). Al_2TiO_5 (80 wt%)–mullite–ZrO_2 composites which combined good mechanical strength (55 MPa), low thermal expansion ($\alpha_{20\text{-}1000\,C} < 1 \times 10^{-6}\,K^{-1}$) and excellent thermal stability were obtained by reaction and sintering of powder mixtures containing both $ZrSiO_4$ and MgO.

1. Introduction

Aluminium titanate, Al_2TiO_5, is a synthetic ceramic material which, owing to its high melting point, low thermal conductivity, low thermal expansion and excellent thermal shock resistance, is considered as a candidate for many structural applications. Thus it is being tested as an insulating material in combustion engines, e.g. as portliner in the cylinder head, piston head, manifold, lining of turbochargers, swirl chamber and valve insulation [1]. Nevertheless, up to now, only one component, namely the engine portliner, was put in series. This is, above all, due to the poor mechanical properties of the materials based on aluminium titanate available at this time [1, 2]. For that reason, one of the main goals of research on aluminium titanate is the improvement of its mechanical properties.

The overall properties of polycrystalline aluminium titanate ceramics are strongly determined by its microstructure which is usually characterized by microcracking along the grain boundaries. This microcracking phenomenon takes place during cooling from the sintering temperature, owing to the unusually strong pronounced anisotropy in thermal expansion of the orthorhombic β–Al_2TiO_5 crystallites ($\alpha_a = -2.9$, $\alpha_b = 10.3$, $\alpha_c = 20.1 \times 10^{-6}\,K^{-1}$ [3]). The presence of these microcracks determines, on the one hand, the low thermal expansion and thermal conductivity of polycrystalline Al_2TiO_5, but on the other hand, also its moderate mechanical strength. Therefore, the approach of strengthening aluminium titanate by reducing its grain size below a critical value where no more microcracking occurs [4] succeeds in strengthening Al_2TiO_5 but is inherently accompanied by an undesired increase in thermal expansion and therefore decrease in thermal shock resistance. Thus, the approach of introducing dispersed particles, which are expected to limit the length of microcracks formed during cooling to a certain tolerable amount and to impede its propagation when mechanically loaded, seems to be more suitable to improve the mechanical strength of Al_2TiO_5 without deterioring its favourable thermomechanical properties.

Nevertheless, the latter assumption holds only for small volume fractions of second phases which have to be located in the grain boundaries or triple points of the aluminium titanate ceramics. To fulfil this requirement the reaction sintering route seems to be very convenient, because *in situ* formed particles are more likely to be located at the triple points rather than enclosed in Al_2TiO_5 grains.

In a former work, Pena *et al.* [5] showed that Al_2TiO_5(80 wt%)/mullite–ZrO_2 composites, obtained by reaction sintering of $Al_2O_3/TiO_2/ZrSiO_4$ powder mixtures exhibit an up to ten times higher bending strength than the monophasic Al_2TiO_5. However, the samples turned out to be unstable in the temperature range 1000 to 1200° C [6]. The aim of the present work was two-fold: (a) to study the influence of the second-phase content in Al_2TiO_5 composites prepared by reaction sintering, and (b) to stabilize the Al_2TiO_5 matrix by means of the addition of a small amount of MgO to the starting powders.

2. Experimental details

2.1. Compositions

Two sets of compositions, the AT-series and the MAT-series, were formulated. The Al_2TiO_5 content after complete reaction varies in both series from 100

0022–2461/90 $03.00 + .12

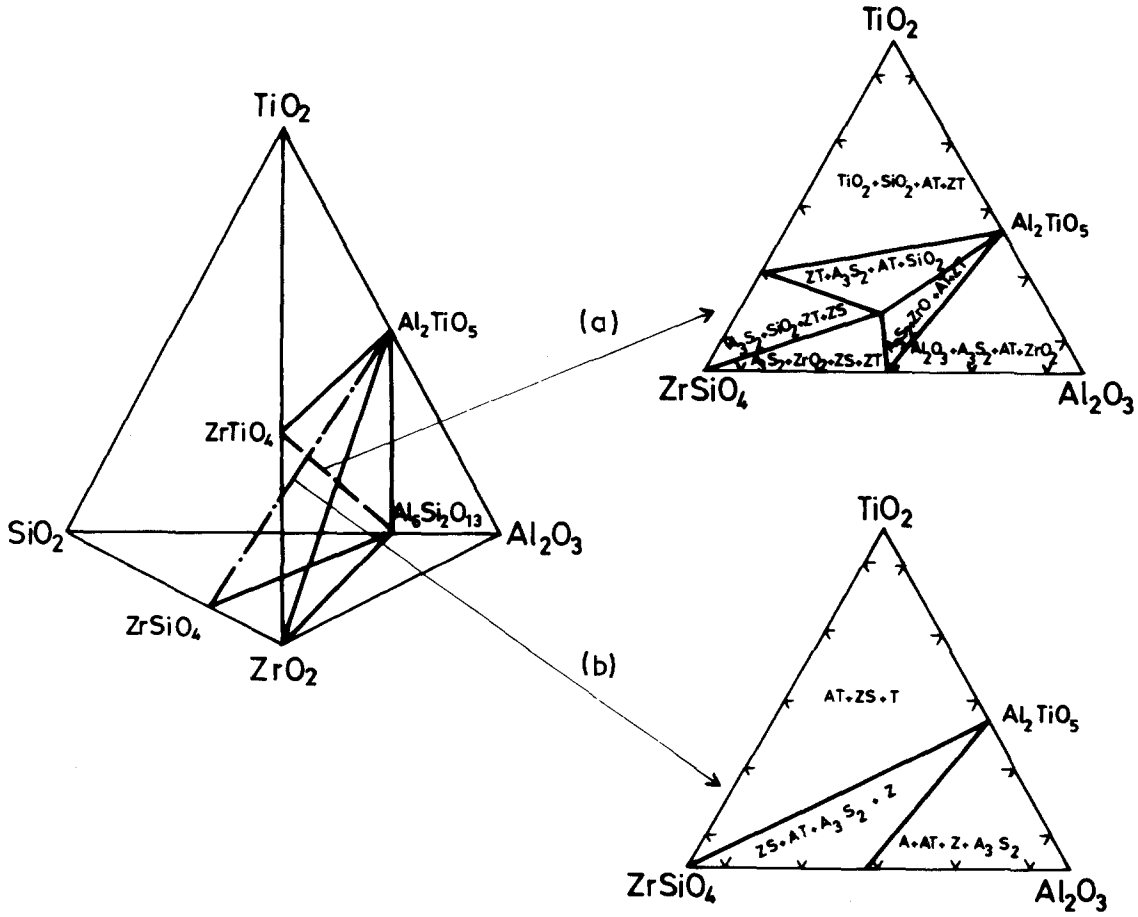

Figure 1 Solid state relationships in the quaternary system Al_2O_3–TiO_2–SiO_2–ZrO_2; (a) $T > 1450°C$, (b) $1285 < T < 1450°C$.

to 80 wt % but the MAT-series also contains 2 wt % MgO. The samples were labelled AT100, AT90, AT80 and MAT100, MAT90, MAT80 respectively, where 100, 90, 80 indicates the weight percentage of Al_2TiO_5 and "M" indicates MgO addition.

AT100 was synthesized according to the reaction

$$Al_2O_3 + TiO_2 \rightarrow Al_2TiO_5 \quad (1)$$

and AT90 and AT80 were formulated according to

$$(3 + x)Al_2O_3 + xTiO_2 + 2ZrSiO_4 \rightarrow xAl_2TiO_5 + Al_6Si_2O_{13} + 2ZrO_2 \quad (2)$$

where $x = 33.7$ and 17, respectively. In an analogous way MAT100 was formulated according to the reaction

$$0.9Al_2O_3 + 1.1TiO_2 + 0.1MgO \rightarrow Al_{1.8}Mg_{0.1}Ti_{1.1}O_5 \quad (3)$$

and MAT90 and MAT80 according to

$$(3 + 0.9y)Al_2O_3 + 1.1yTiO_2 + 2ZrSiO_4 + 0.1MgO \rightarrow yAl_{1.8}Mg_{0.1}Ti_{1.1}O_5 + Al_6Si_2O_{13} + 2ZrO_2 \quad (4)$$

where $y = 32.7$ and 17, respectively. However, Reaction 4 has only a hypothetical character because one of the objectives of the present work was just to establish the existence of the solid solution of MgO in Al_2TiO_5 in the presence of other phases such as zirconia and mullite.

2.2. Phase equilibria

The validity of Reactions 1 to 4 can be seen from the corresponding phase diagrams. Thus, the equilibrium diagrams Al_2O_3–TiO_2 [7] and Al_2O_3–TiO_2–MgO [8] indicate that in the range of temperatures studied in this work (1350 to 1500° C), Al_2TiO_5 and Al_2TiO_{5ss} (ss = solid solution) are the only stable phases in compositions AT100 and MAT100, respectively.

The solid state relationships in the plane zircon–alumina–titania of the quarternary system Al_2O_3–TiO_2–SiO_2–ZrO_2 are depicted in Figs 1 and 2 as constructed from previously reported data [9, 10]. Solid state compatibilities in this plane change at 1450° C. Below 1450° C $ZrSiO_4$ is compatible with Al_2TiO_5 and above this $ZrTiO_4$ is compatible with mullite [11, 12]. Nevertheless, because the compositions AT90 and AT80 are located in the plane Al_2TiO_5–mullite–ZrO_2 the phase composition should not be affected by this compatibility change. Both compositions are located in the primary phase field of Al_2TiO_5 and liquid should not appear below 1575° C [9]. Below 1285° C [13], as indicated in Fig. 2, compatibilities change again due to the decomposition of Al_2TiO_5, now being Al_2O_3–TiO_2–$ZrTiO_4$–$Al_6Si_2O_{13}$.

The quinary system, MgO–Al_2O_3–TiO_2–SiO_2–ZrO_2 is sketched in Fig. 3. Due to an extended solid solution between Al_2TiO_5 and $MgTi_2O_5$, compositions MAT90 and MAT80 are situated in the pseudoternary system Al_2TiO_{5ss}–$Al_6Si_2O_{13ss}$–ZrO_{2ss} for temperatures higher than 1285° C.

2.3. Preparation techniques and experimental methods

According to Reactions 1 to 4, appropriate quantities of Al_2O_3 (Alcoa Ct 3000 SG, BET surface 8 $m^2 g^{-1}$,

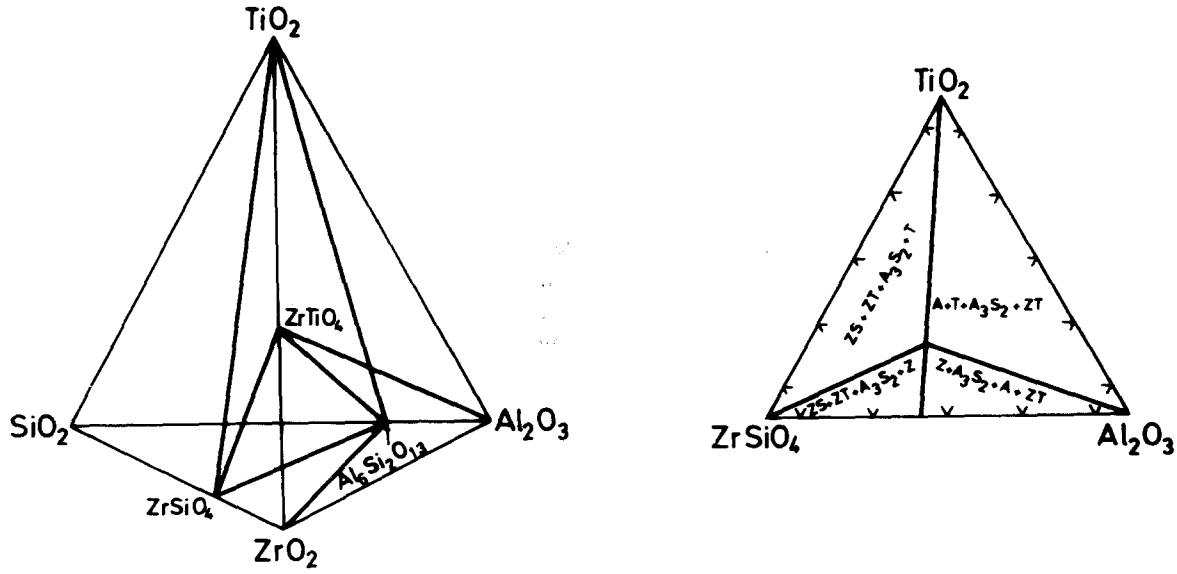

Figure 2 Solid state relationships in the quaternary system Al_2O_3–TiO_2–SiO_2–ZrO_2, $T < 1285°C$.

$d_{50} = 0.5\,\mu m$, phase composition corundum), TiO_2 (Merck 808, BET surface $9\,m^2\,g^{-1}$, $d_{50} = 0.40\,\mu m$, phase composition anatase), $ZrSiO_4$ (Opacir Quiminsa, BET surface $7\,m^2\,g^{-1}$, $d_{50} = 1.1\,\mu m$, phase composition zircon) and MgO (Probus, phase composition periclase, brucite) were mixed by attrition milling with Mg–PSZ balls in isopropanol. After drying and sieving, the powders were isostatically pressed to rods of approximately 4 mm diameter. The chemical analyses of the as-milled powders are shown in Table I.

A differential thermal analysis (DTA) curve of all compositions was recorded with a thermal analyser (Mettler type) between room temperature and 1500° C using a heating rate of $10\,K\,min^{-1}$. The shrinkage behaviour during constant heating was established in a dilatometer (Adamel Lhomargy) using green rods of 4 mm diameter and 10 mm height. With the aim of facilitating the interpretation of DTA and dilatometric experiments, several samples were heated to 1000 or 1280° C, respectively, at $10\,K\,min^{-1}$ and subsequently air-quenched.The phase content determined by X-ray diffraction (XRD) can be seen from Table II.

Green specimens were fired in an electric temperature-controlled furnace heated by Superkanthal elements at temperatures ranging from 1350 to 1500° C. The phase content was determined by X-ray diffraction using the Cu$K\alpha$ radiation of a Philips 1010 diffractometer with nickel filter. The bulk density of the fired samples was measured by the water displacement method. The modulus of rupture was measured in an Instron machine using three-point load, a 20 mm span, and a cross-head speed of $0.5\,mm\,min^{-1}$ on rods of 4 mm diameter. The microstructure was characterized by reflected light microscopy (RLM) and scanning electron microscopy (SEM) on polished and chemically etched surfaces (HF 15 vol %, 3 min).

Specimens fired at 1400° C for 2 h and at 1500° C for 1 h were annealed at 1150° C for several periods up to 200 h. Several authors had reported that decomposition of aluminium titanate takes place at 1150° C with maximum velocity [6, 14]. The thermal stability, v, of these samples was estimated in terms of the Al_2TiO_5 fraction defined as

$$v = c_{AT}/(c_{AT} + c_T) = I_{AT}/(I_{AT} + K^{-1} I_T)$$

where c_{AT} and c_T represent the weight fraction of β-Al_2TiO_5 and TiO_2 (rutile), respectively. The X-ray intensities, I_{AT} and I_T, were determined from the (0 2 3) peak of Al_2TiO_5 and the (1 0 1) peak of TiO_2. K was calibrated as $K = 0.77 \pm 0.098$. It should be noted that v can vary between 0, completely decomposed, and 1, corresponding to stable.

The expansion behaviour of sintered specimens between room temperature and 1000° C during heating and cooling was established in an inductive dilatometer with Al_2O_3 support. The experiments were run at $2\,K\,min^{-1}$ heating rate on specimens of 20 mm height. The dilatometric curves obtained in that way were corrected using theoretical values of Al_2O_3.

TABLE I Chemical analysis after attrition milling

	AT100	AT90	AT80	MAT100	MAT90	MAT80
Al_2O_3	55.0	54.0	52.8	48.4	47.5	47.2
TiO_2	43.4	39.5	36.4	47.0	43.1	40.2
ZrO_2	0.28	3.73	6.33	0.34	3.43	6.19
SiO_2	0.48	1.90	3.50	0.48	1.90	3.22
MgO	0.067	0.060	0.067	1.97	1.72	1.56
CaO	0.061	0.040	0.048	0.098	0.066	0.062
Fe_2O_3	0.018	0.050	0.030	0.04	0.035	0.033
Na_2O	0.07	0.085	0.085	0.085	0.13	0.085
K_2O	0.01	0.024	0.024	0.024	0.024	0.024
P_2O_5*	0.1	0.1	0.1	0.1	0.1	0.1
Ign. loss	0.7	0.8	0.8	1.2	2.0	1.1

*Low precision.

TABLE II Phase composition of selected compacts after heating at $10\,K\,min^{-1}$ to 1000 and 1280° C and subsequent air-quenching

	1000° C	1280° C
AT100	A, TA, TR	A, TR
AT80	A, TA, TR, ZS	A, TR, ZS, (TA)
MAT100	A, TA, TR, MT_2	AT, TR, A
MAT80	A, TA, TR, ZS, MT_2	A, TR, TA, ZS

A = α-Al_2O_3, TR = TiO_2 rutile, TA = TiO_2 anatase, ZS = $ZrSiO_4$, AT = β-Al_2TiO_5, MT_2 = $(MgTi_2O_5)_{ss}$, Indicate minor phases.

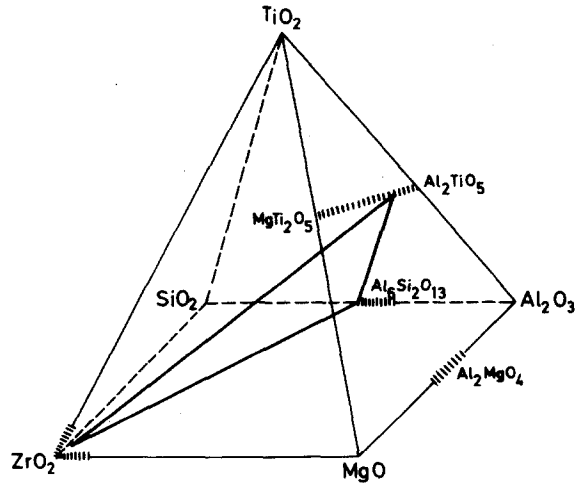

Figure 3 Schematic representation of solid state relationships in the system $MgO-Al_2O_3-TiO_2-SiO_2-ZrO_2$ for $T > 1285°C$.

3. Results and discussion

3.1. Differential thermal analysis

The DTA curve of composition AT100, Fig. 4a, shows only one endothermic peak corresponding to the formation of Al_2TiO_5. With addition of 5 or 10 wt % $ZrSiO_4$ this peak is shifted to 1360 or 1385° C, respectively. This shift in the formation temperature cannot be explained simply with a steric hindrance due to the dispersed $ZrSiO_4$. Rather, it can be assumed that solid solutions are formed of Zr^{4+} and/or Si^{4+} in alumina and/or titania which increase the stability of the reactants and therefore higher temperatures are required for the reaction to take place. The retarding effect of Zr^{4+} on the Al_2TiO_5 formation was reported previously by Ohya *et al.* [14].

In the samples with MgO addition, Fig. 4b, broadening of the endothermic reaction peak at 1345° C and a shift to lower temperatures can be observed. Thus, in MAT100, aluminium titanate formation occurs at approximately 1280° C, and in MAT90 and MAT80 at temperatures slightly above. This can be explained from the fact that the matrix phase with the theoretical composition $Al_{1.8}Mg_{0.1}Ti_{1.1}O_5$ represents a solid solution of Al_2TiO_5 and $MgTi_2O_5$, which exhibits the much lower formation temperature of 920° C [3].

In none of the curves can any peak related to the decomposition of zircon be observed. This can probably be attributed to the fact that the reaction kinetics of zircon decomposition and mullite formation is much slower than that of aluminium titanate formation as reported in a previous work [5].

It is noteworthy that, unless all the starting powders contained TiO_2 in the anatase modification, in most of the samples the aluminium titanate formation takes place from α-Al_2O_3 and rutile, as can easily be seen from Table II. Obviously, only AT80 still contains some residual anatase when the reaction takes place. However, it is not surprising that no evidence for the anatase–rutile transformation can be found in the DTA curves because there is only a 0.5% difference between the lattice energies of anatase and rutile [15]. Furthermore, Table II sustains the accelerating effect of MgO on this phase transformation reported in the literature [15] and suggests a decelerating influence of $ZrSiO_4$.

3.2. Dynamic sintering

During constant-heating-rate sintering, Fig. 5, samples of AT series show quite similar behaviour between room temperature and 1300° C; they exhibit a high densification rate between 1000 and 1300° C. The densification rate of AT100 slows down abruptly at 1320° C, indicating the expansive formation of aluminium titanate. On the contrary, AT90 and AT80 continue shrinking up to temperatures approximately 50° C above, in good agreement with the DTA results, and therefore reach higher end-point densities. The shrinkage curve of AT80, which was recorded up to 1600° C, even shows expansion over a small temperature range which could be attributed to the again expansive reaction between zircon and alumina.

In the MgO series, Fig. 5b, the change in shrinkage rate due to the Al_2TiO_5 formation is much less pronounced. In MAT100 a diminution of shrinkage rate can be observed between 1270 and 1320° C and between 1300 and 1350° C in samples MAT90 and MAT80. After that interval, as opposed to the AT series, strong densification continues but slows down in the case of MAT90 and MAT90 above 1400° C. The latter observation indicates that the expansive reaction between Al_2O_3 and $ZrSiO_4$ is also favoured due to the addition of MgO.

From DTA and dynamic sintering experiments it is clear that addition of 2 wt % MgO to the Al_2O_3/TiO_2

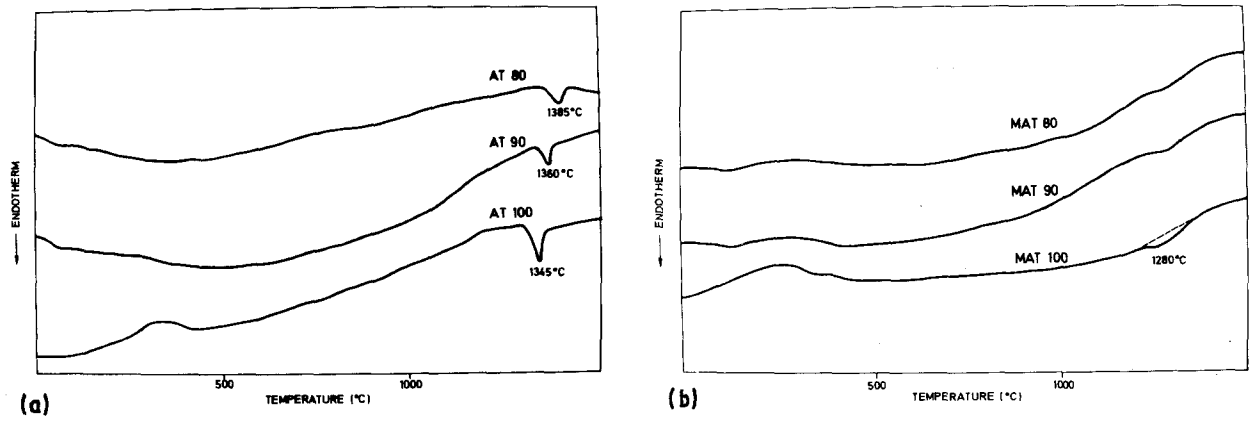

Figure 4 Differential thermal analysis: (a) AT-series, (b) MAT-series. Heating rate 10° C min^{-1}.

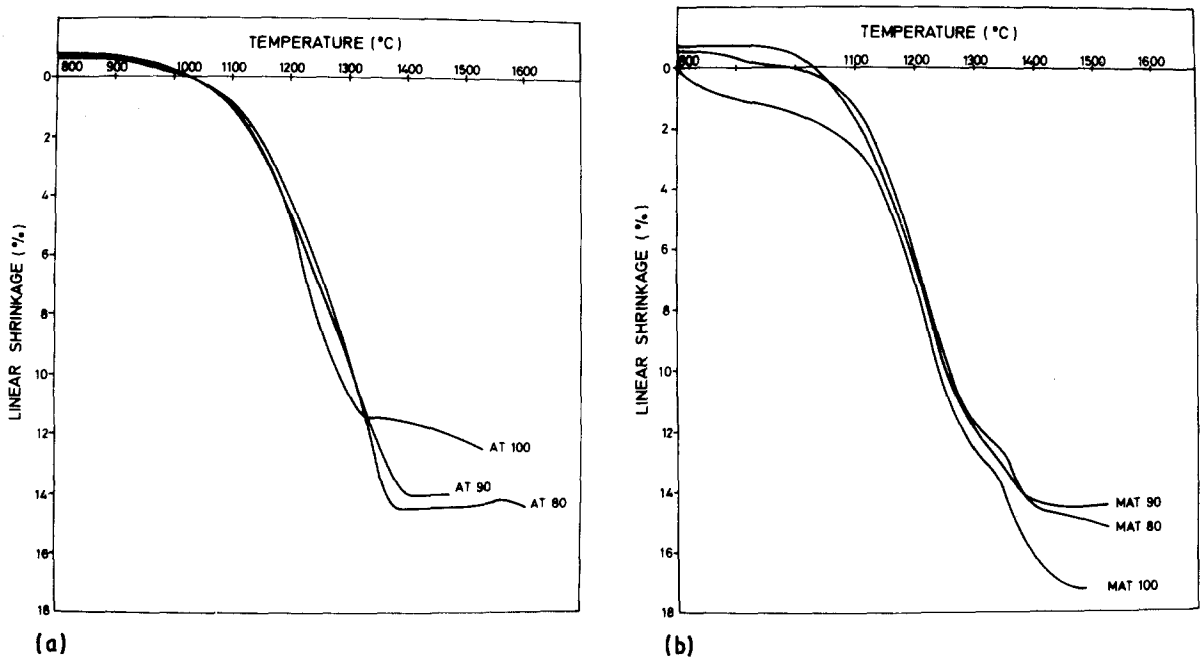

Figure 5 Constant-heating-rate sintering of the green and isopressed samples: (a) AT-series, (b) MAT-series. Green density 60%, heating rate 10° C min^{-1}.

starting powder produces Al_2TiO_5 formation at lower temperatures and enhances sintering. Addition of 5 or 10 wt % $ZrSiO_4$ shifts the Al_2TiO_5 formation to higher temperatures but also favours densification. However, no further increase of densification is observed when MgO is added to the $Al_2O_3/TiO_2/ZrSiO_4$ mixture. Thus, if one compares the shrinkages reached at 1500° C the sequence

MAT100 > AT90, AT80, MAT90, MAT80 > AT100

can be observed. To explain this effect, it has to be taken into account that in all samples, contrary to the respective phase-diagram predictions, small amounts of liquid phase are present, as has been found by transmission electron microscopy (TEM) [16]. This glassy phase is formed due to the presence of impurities which are introduced through raw materials or the milling process (Table I) even in sample AT100. The addition of a small amount of MgO favours the liquid formation and reduces its viscosity at high temperatures. Also the step-wise decomposition of $ZrSiO_4$, accompanied by formation of a transitory SiO_2-rich glassy phase [17], accelerates the densification in comparison to AT100. But in MAT90 and MAT80 no further increase in densification is observed because MgO also enhances the expansive formation of mullite and ZrO_2.

3.3. Phase evolution during sintering

The phase content of the sintered specimens as a function of sintering temperature is depicted qualitatively in Fig. 6. Sintering AT100 for 2 h at temperatures between 1350 and 1450° C yielded aluminium titanate with some residual Al_2O_3 and TiO_2. In a TEM study of these samples it was observed that the residual Al_2O_3 and TiO_2 particles are enclosed in large Al_2TiO_5 grains [16] and long diffusion times would be necessary to complete the reaction. After 2 h sintering at 1500° C, only a small amount of Al_2O_3 and no TiO_2 were detected by XRD, which could also indicate deviations from stoichiometry. Conversely, only aluminium titanate was found in MAT100 at all sintering temperatures. This is illustrating again the favourable effect of MgO on the Al_2TiO_5 formation.

In samples AT90 and AT80, $ZrSiO_4$ decomposes forming $ZrTiO_4$ as an intermediate compound. Sintering temperatures as high as 1500° C were necessary to dissociate this compound, i.e. to complete the Al_2TiO_5 formation. In AT80, a small amount of mullite is formed at 1425° C. The mullite formation increases with sintering temperature but the temperature has to be raised to 1500° C to yield complete decomposition of $ZrTiO_4$ and $ZrSiO_4$. After sintering at 1500° C, Al_2TiO_5, zirconia, mullite plus alumina are found. This excess in alumina could indicate that AT80 composition is not really located in the compatibility plane Al_2TiO_5–$Al_6Si_2O_{13}$–ZrO_2 but is shifted to the compatibility tetrahedron Al_2TiO_5–ZrO_2–$Al_6Si_2O_{13}$–Al_2O_3 (Fig. 1) due to either small deviations because of impurities or solid solution effects. Another plausible explanation would be that the reaction has not yet reached equilibrium, e.g. mullite is not formed entirely and therefore Al_2O_3 and an SiO_2-rich glassy phase are present in the sample. The existence of this glassy phase was, in fact, corroborated by electron microscopy (Fig. 7).

In the MgO-doped samples MAT90 and MAT80, much lower temperatures are required to yield complete $ZrSiO_4$ decomposition. The accelerating effect of MgO on the decomposition of zircon has already been reported by Miranzo *et al.* [18]. In contrast to samples AT90 and AT80, $ZrTiO_4$ was never detected. In MAT80, mullite is formed at temperatures about 75° C lower than in the corresponding sample without MgO addition. When the temperature is raised to 1500° C no further mullite is found and an appreciable amount of glassy phase was detected by SEM (Figs 7, 8). These facts indicate that when temperature is increased from 1425 to 1500° C, a liquidus surface is

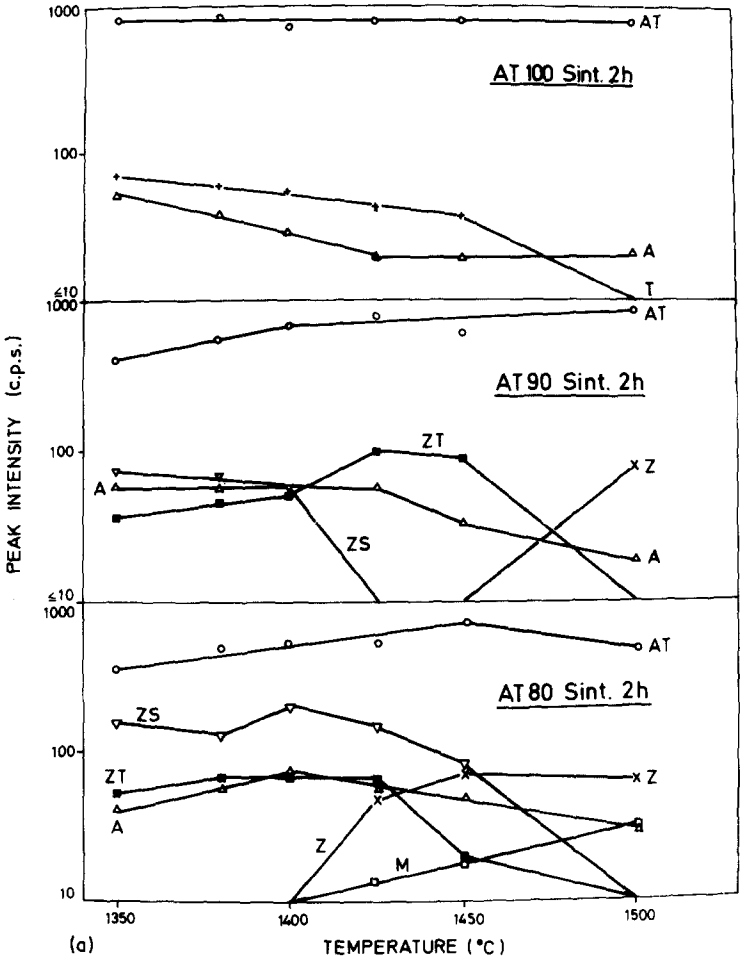

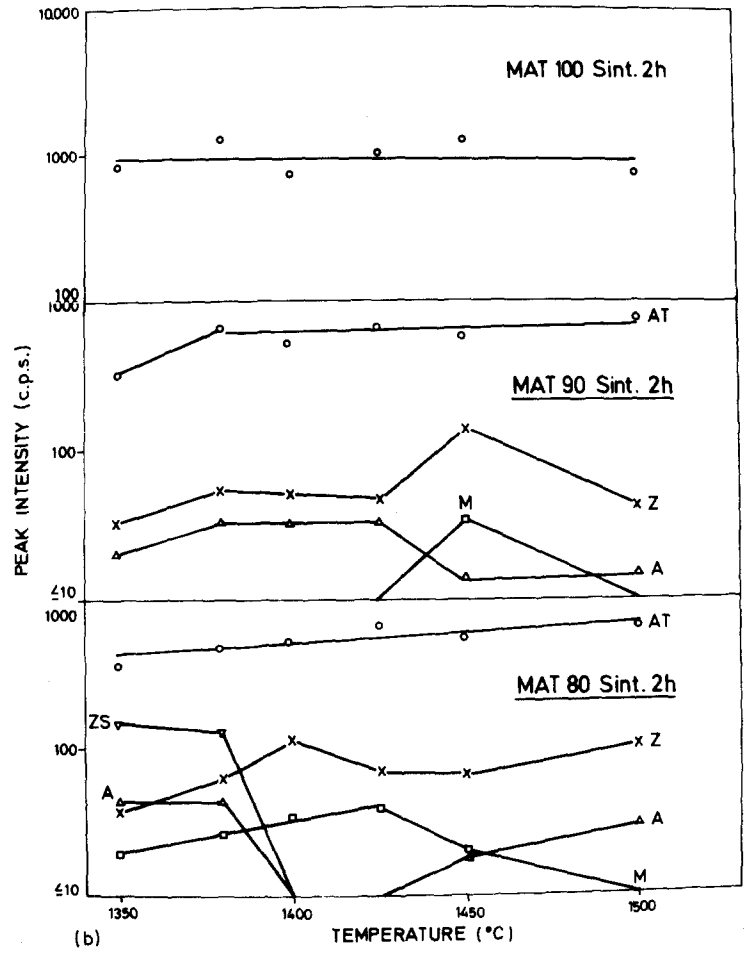

Figure 6 Phase composition–sintering temperature plots as indicated from the following XRD peaks: (a) AT-series, (b) MAT-series; AT = β-Al_2TiO_5(0 2 3), A = α-Al_2O_3(1 1 3), T = TiO_2 rutile (1 0 1), M = mullite (1 2 1), Z = ZrO_2(1 1 $\bar{1}$), ZS = $ZrSiO_4$(2 0 0), ZT = $ZrTiO_4$(1 1 1).

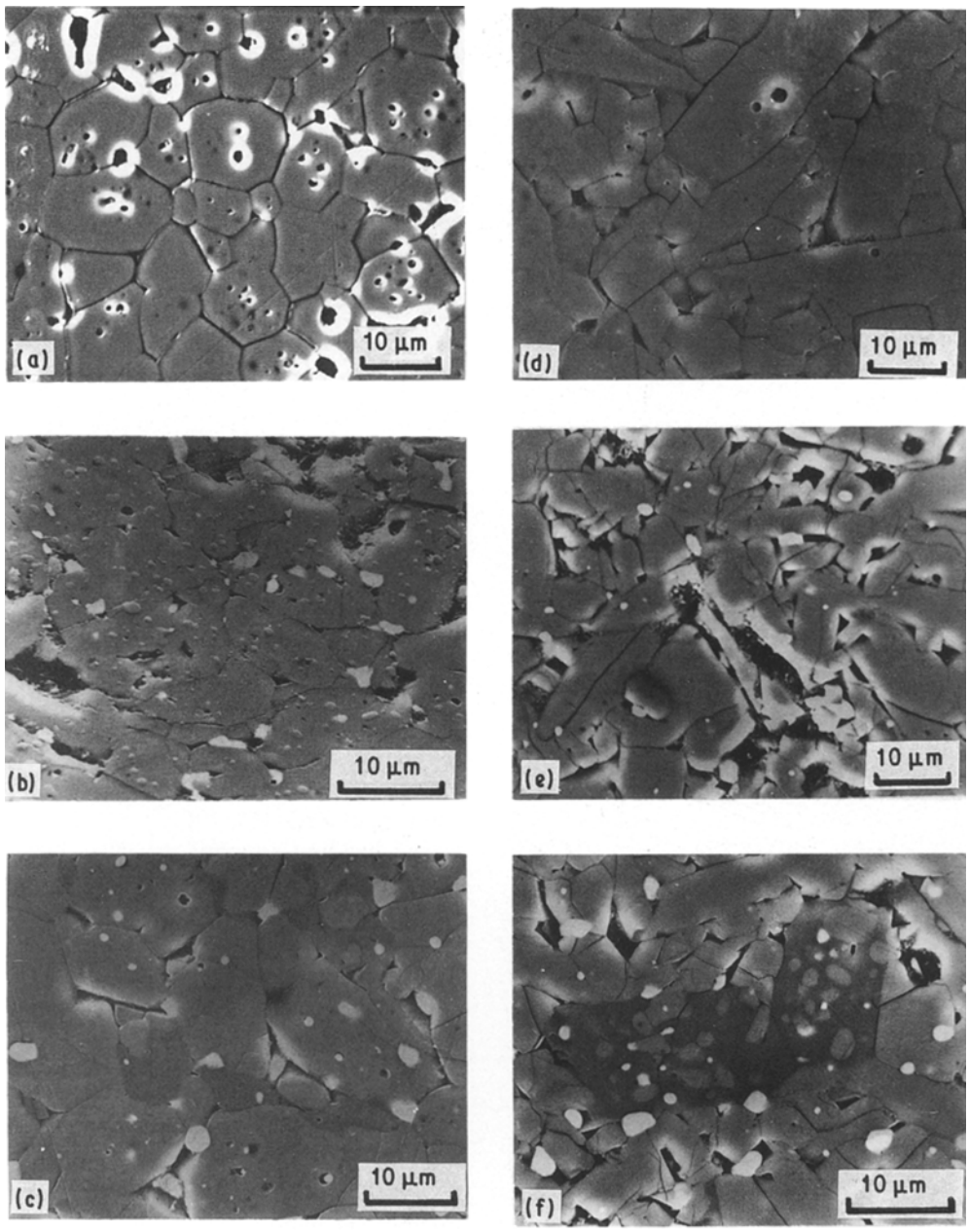

Figure 7 Scanning electron micrographs of polished and etched surfaces: (a) AT100, (b) AT90, (c) AT80, 1500° C; (d) MAT100, (e) MAT90, (f) MAT80, 1450° C.

crossed in the quinary phase diagram Al_2O_3–TiO_2–SiO_2–ZrO_2–MgO.

3.4. Microstructure

The microstructures of the AT-series (1500° C) and MAT-series (1450° C) are compared in Fig. 7. As can be observed, the sintered samples are formed by an Al_2TiO_5 matrix with zirconia and mullite as second phases which are mainly dispersed in grain boundaries and triple points. The zirconia particles have a grain size of $\leqslant 3$ μm. Microcracks can be observed along the grain boundaries. The micrographs in Figs 7 and 8 sustain the existence of a small amount of glassy phase in all samples being predominantly located at triple points. Energy-dispersive X-ray microanalysis (EDX) revealed that these glassy pockets are mainly composed of silicon accompanied by minor quantities of zirconium, magnesium and calcium. These impurities come from the raw materials or are introduced through the milling process (Table I). It is evident from Fig. 7 that the amount of glassy phase increases with the introduction of $ZrSiO_4$ or $ZrSiO_4$ and MgO.

Although the samples of the MAT-series were sintered at temperatures 50° C lower, no significant difference in aluminium titanate grain size can be appreciated. However, there is a remarkable difference in the habit of the Al_2TiO_5 grains. In the AT-series, Al_2TiO_5 grains are almost equiaxed, e.g. aspect ratio = 1.4 ± 0.5 in AT100. On the contrary, in the MAT-series, the longer, needle-like shape of the Al_2TiO_5 phase is observed, e.g. 2.1 ± 1.1 in MAT100. It can be observed that the introduction of dispersed particles does not produce a reduction in grain size either. The habit of mullite, the large, dark grains in Figs 7c and d, is different in AT80 and MAT80, indicating growth in presence of liquid phase in MAT80.

3.5. Density and mechanical properties

The densities of specimens sintered for 2 h in the

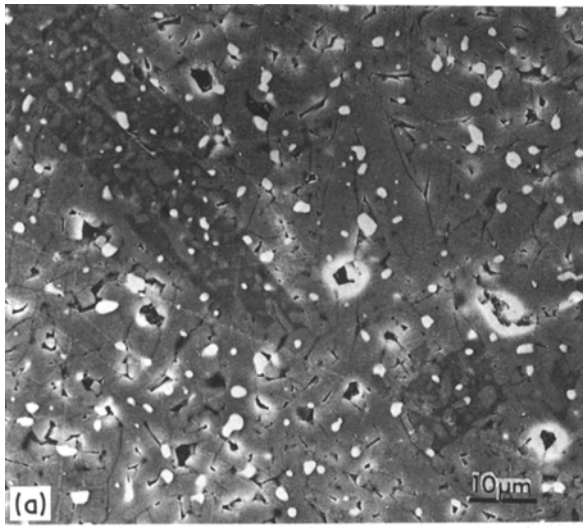

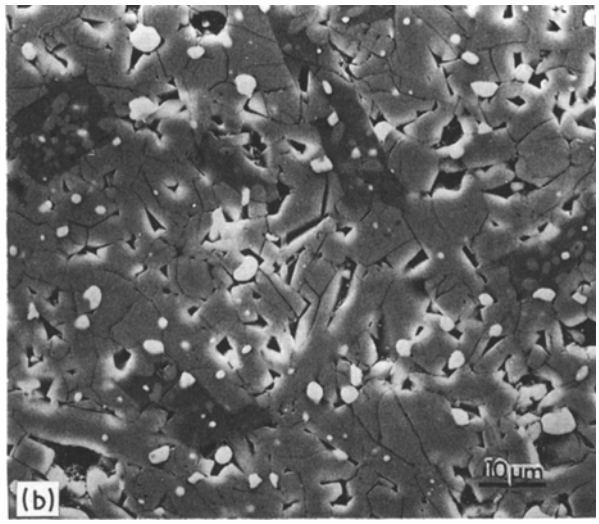

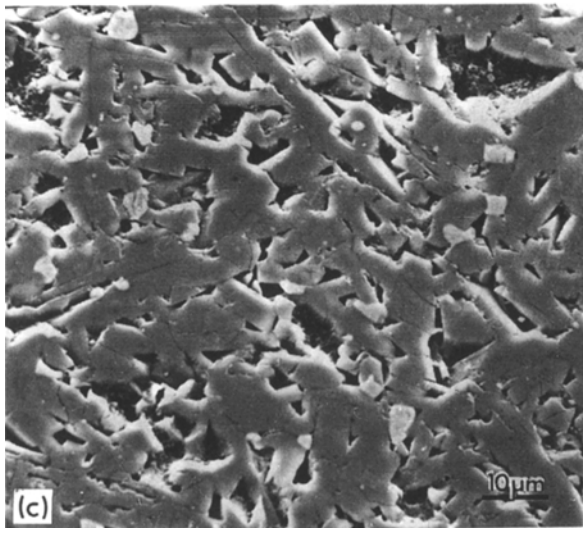

Figure 8 Scanning electron micrographs of MAT80, sintered for 2 h at (a) 1425° C, (b) 1450° C, (c) 1500° C.

temperatures 1350 to 1500° C are depicted in Fig. 9. Relative density does not decrease with increasing sintering temperature, as could be concluded falsely from the bulk density–temperature plot, because phase composition changes from high-density phases at low temperatures to phases with a lower density at higher temperatures. Because no quantitative phase analysis has been done it is not possible to calculate the relative densities at all temperatures studied. In the cases where the phase compositions were obtained as expected from the phase diagrams (AT100 1500° C, MAT100 1350 to 1500° C, AT80 1500° C, MAT80 1425° C) densities > 96% were estimated. The trends suggested by the dynamic sintering experiments are confirmed if one compares the densities obtained at 1450 or 1500° C. Thus, it should be emphasized that the addition of $ZrSiO_4$ and an appropriate excess of Al_2O_3 to the starting powder is quite effective in generating ZrO_2 particles and presents the advantage of enhancing densification contrary to the direct addition of ZrO_2 [14, 19].

The bending strength (σ_f) is plotted against sintering temperature in Fig. 10. The σ_f value in all specimens decreases linearly with increasing sintering temperature owing to a decrease in microcracking [20, 21]. The introduction of dispersed phases produces both in AT- and MAT-series an increase in bending strength which is higher in the samples with addition of 10 wt % $ZrSiO_4$ (AT80, MAT80) than in those with only 5 wt % $ZrSiO_4$ (AT90, AT90). Because this strengthening effect is observed at all temperatures it must be concluded that the nature of the dispersed phases is of secondary importance. Consequently, the hypothesis that strengthening in this type of material is caused by a change in microcrack habit induced by the tetragonal to monoclinic transformation of ZrO_2 [5, 22] must be rejected. Fig. 7 illustrates furthermore that no significant reduction of grain size is achieved by the introduction of dispersed particles. Thus, it can be concluded that these particles are above all effective in strengthening Al_2TiO_5 because, located mainly at grain boundaries and triple points, they can act as a hindrance to crack propagation, both during cooling from sintering temperature and when the specimens are mechanically loaded.

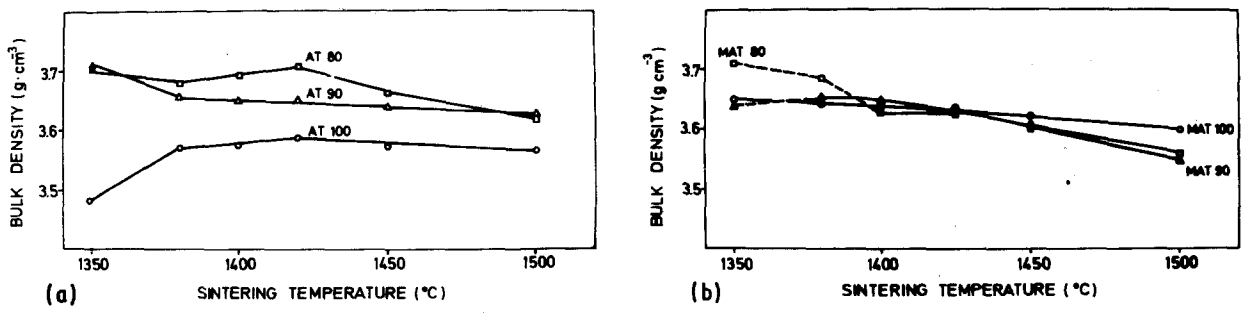

Figure 9 Bulk density–sintering temperature plots: (a) AT-series, (b) MAT-series.

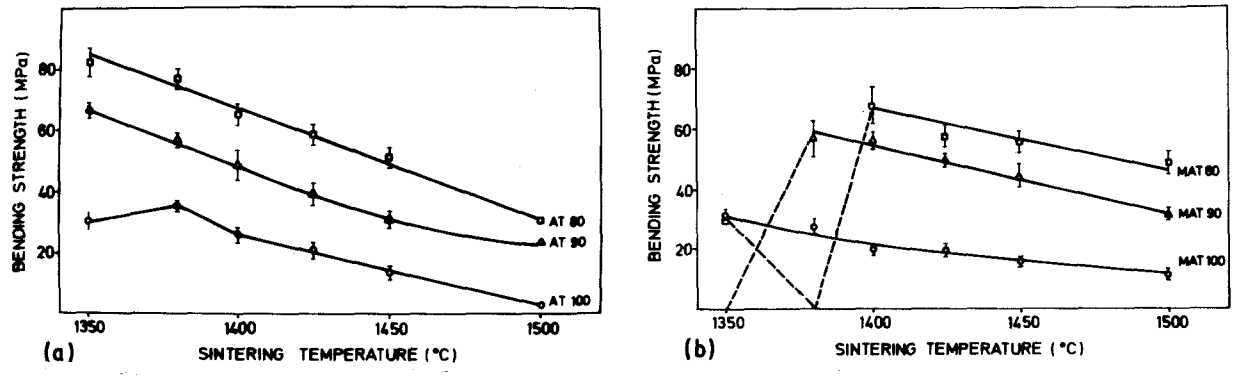

Figure 10 Bending strength–sintering temperature plots: (a) AT-series, (b) MAT-series. Soaking time = 2 h.

Comparing AT- and MAT-series, a small additional effect on strength due to MgO addition can be observed, as can be seen more clearly from Fig. 11. It is commonly assumed that MgO solid solutions in Al_2TiO_5 reduce the anisotropy in thermal expansion and therefore the amount of microcracking [23]. This would explain the slightly higher strength of the MgO-containing samples. But, it cannot be ruled out that the microstructural change produced by MgO addition also plays an important role. As mentioned above, the MgO-free samples present nearly equiaxial microstructures, whereas the MgO-doped specimens possess a longish shape and therefore offer more resistance to crack opening due to grain interlocking in the crack wedge.

Nevertheless, in the MAT-series it was not possible to reduce sintering unlimitedly in order to get higher strength. Samples MAT80 and MAT90 showed pronounced macroscopic cracking over the whole sample at 1380 and 1350° C, respectively (compare Fig. 12). Because this phenomenon was found to be reproducible, the strength of these samples was considered to be zero. A similar phenomenon was reported by Hamano *et al.* [24] during sintering of presynthesized Al_2TiO_5 at 1400° C. However, no convincing explanation has been found until today.

3.6. Thermal stability

The thermal stability of selected samples of both series is depicted as a function of sintering conditions and ageing time in Fig. 13. Care has to be taken with the interpretation of the data from the multiphasic samples because solid state compatibilities change in the quaternary system when Al_2TiO_5 decomposes (Fig. 2) and $ZrTiO_4$ can be formed which could falsify the decomposition data. In fact, small amounts of $ZrTiO_4$ were found in AT90, AT80, MAT90, and MAT80 after long-term treatment. Taking into account that the maximum amount of $ZrTiO_4$ to be formed is determined by the ZrO_2 content, a possible error of $\Delta v = 11\%$ was calculated, which appears to be tolerable.

In the AT-series, the eutectoid decomposition of Al_2TiO_5 proceeds rapidly as is indicated by the steep slope of the decomposition curves. No appreciable nucleation period can be observed. All samples without MgO addition show complete decomposition of the Al_2TiO_5 matrix to TiO_2 and Al_2O_3 after 24 h. Addition of $ZrSiO_4$ does not show any significant influence on stability. It is known that ZrO_2 does not stabilize aluminium titanate, whereas SiO_2 is reported to be a very effective stabilizing agent [25]. Therefore, it must be concluded that in the compositions studied in the present work, SiO_2 does not form solid solutions in Al_2TiO_5.

The microstructures of sample AT100 (1500° C, 1 h) after annealing for several times at 1150° C are compared in Fig. 14. After 1.5 h, nucleation of TiO_2 inside the Al_2TiO_5 grains can be observed (Fig. 14a). These TiO_2 nuclei are mainly associated to small intergranular pores. After 6 h treatment (Fig. 14b) large corundum (dark) and rutile grains (white) can be observed, mainly located at the grain boundaries. After 24 h, the sample is entirely decomposed (Fig. 14d)

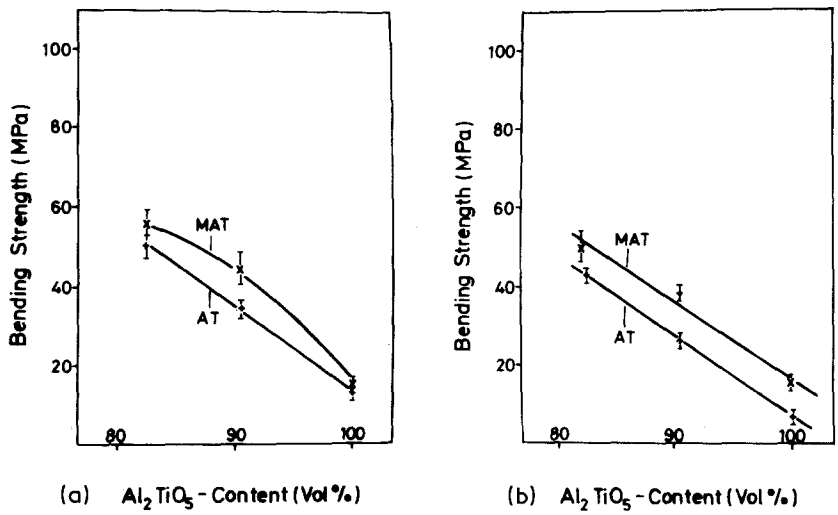

Figure 11 Bending strength–Al_2TiO_5 content plots for two different sintering conditions: (a) 1450° C, 2 h; (b) 1500° C, 1 h.

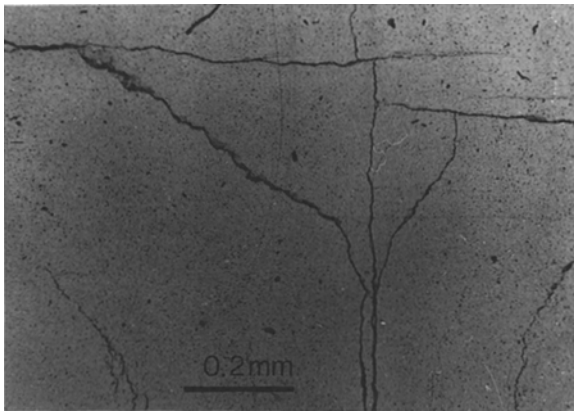

Figure 12 Optical micrograph of MAT80 after sintering at 1380° C for 2 h showing strong microcracking.

and the microstructure consists of Al_2O_3 plates embedded in a TiO_2 matrix.

On the other hand, the MgO-doped samples were much more stable than the AT-series. An induction period of about 200 h in MAT100 and 100 h in MAT90 and MAT80 is appreciated before decomposition begins. Only a small difference in stability is found between MAT90, MAT80 and MAT100 in Fig. 13a. However, there is a strong influence of sintering temperature. The multiphasic samples MAT90 and MAT80 are much less stable when sintered at 1500° C due to the presence of an appreciable amount of glassy phase which can dissolve some part of MgO. That is, MgO is effective in stabilizing Al_2TiO_5 not only in monophasic samples [25] but also in the presence of mullite and/or zirconia when the appropriate sintering conditions are chosen.

3.7. Thermal expansion

The thermal expansion behaviour of sintered specimens is depicted in Fig. 15. The samples were selected based upon the criterion to have comparable phase compositions (reaction sintering process completed) and a comparable amount of glassy phase. All samples show low thermal expansion and hysteresis between heating and cooling which is typical for materials based on aluminium titanate. Sample AT100 exhibits a slightly negative coefficient of thermal expansion, $\alpha_{25\,\text{to}\,1000\,\text{C}} \approx -0.4 \times 10^{-6}\,\text{K}^{-1}$, which is becoming positive with increasing content of second-phase AT90: $\alpha_{25\,\text{to}\,1000\,\text{C}} \approx +0.3 \times 10^{-6}\,\text{K}^{-1}$, AT80: $\alpha_{25\,\text{to}\,1000\,\text{C}} \approx +0.8 \times 10^{-6}\,\text{K}^{-1}$. The introduction of MgO produced in all compositions a reduction of α which varies in the MAT-series between $-1 \times 10^{-6}\,\text{K}^{-1}$ (MAT100) and 0 (MAT80).

However, there is a remarkable difference in the influence exerted by the second phases. In the MAT-series, the hysteresis area measured in terms of arbitrary units is constant, ≈ 80 arb. units, whereas in the AT-series, the hysteresis area is reduced from 100 arb. units in MAT100 to about 30 arb. units in AT90 and AT80.

4. Conclusions

It has been shown that reaction sintering of $Al_2O_3/TiO_2/ZrSiO_4$ powder mixtures is a successful way of producing aluminium titanate ceramics containing dispersed phases.

The presence of 5 to 10 wt % $ZrSiO_4$ enhances the densification of these materials and shifts the Al_2TiO_5 formation to higher temperatures. During the reaction-sintering process, $ZrSiO_4$ decomposes forming $ZrTiO_4$ as a transitory phase. Temperatures higher than 1450° C are necessary to dissociate the compound yielding Al_2TiO_5, mullite, and ZrO_2.

The introduction of 5 and 10 wt % $ZrSiO_4$, producing dispersed particles in the triple points, yields an additional increase of 20 and 40 MPa at all sintering temperatures. In the temperature range 1350 to 1500° C, σ_f values decrease linearly with increasing sintering temperature.

The simultaneous presence of Zr^{4+} and Si^{4+} does not show any stabilizing effect on aluminium titanate.

In the presence of up to 20 wt % mullite and ZrO_2, the coefficient of thermal expansion of specimens sintered at 1500° C is still smaller than $1 \times 10^{-6}\,\text{K}^{-1}$.

Introduction of 2 wt % MgO to the $Al_2O_3/TiO_2/ZrSiO_4$ starting mixture does not produce any further increase in densification but accelerates the reactions taking place, that is, Al_2TiO_5 formation and $ZrSiO_4$ decomposition. In the presence of MgO, $ZrTiO_4$ does not appear. Thus, Al_2TiO_5–mullite–ZrO_2 composites can be obtained at 1425° C. Temperatures should not be raised to 1500° C because this produces an appreciable amount of glassy phase accompanied by the disappearance of mullite.

The bending strength of the MgO-containing samples shows qualitatively the same dependence on the $ZrSiO_4$ fraction as the specimens without MgO. In samples sintered in the temperature range 1425 to 1500° C, there is furthermore a small additive

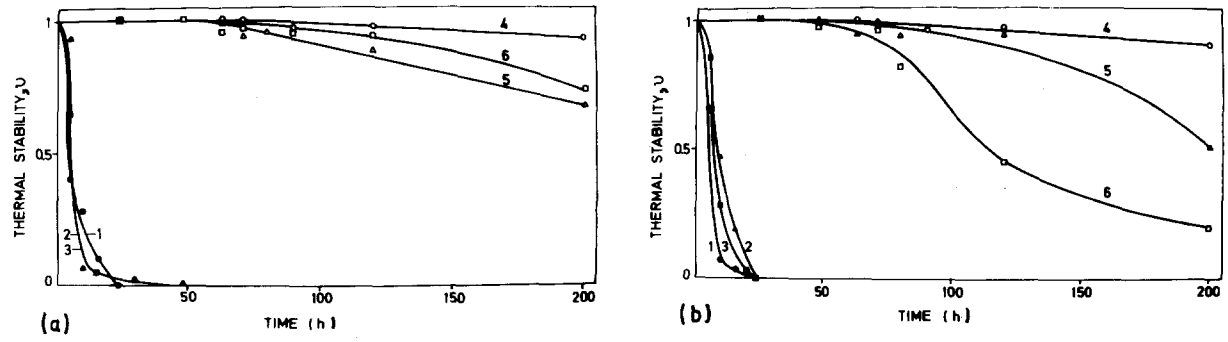

Figure 13 Thermal stability of sintered specimens–annealing time at 1150° C of samples sintered at (a) 1450° C, 2 h, (b) 1500° C, 1 h. (1) AT100, (2) AT90, (3) AT80, (4) MAT100, (5) MAT90, (6) MAT80.

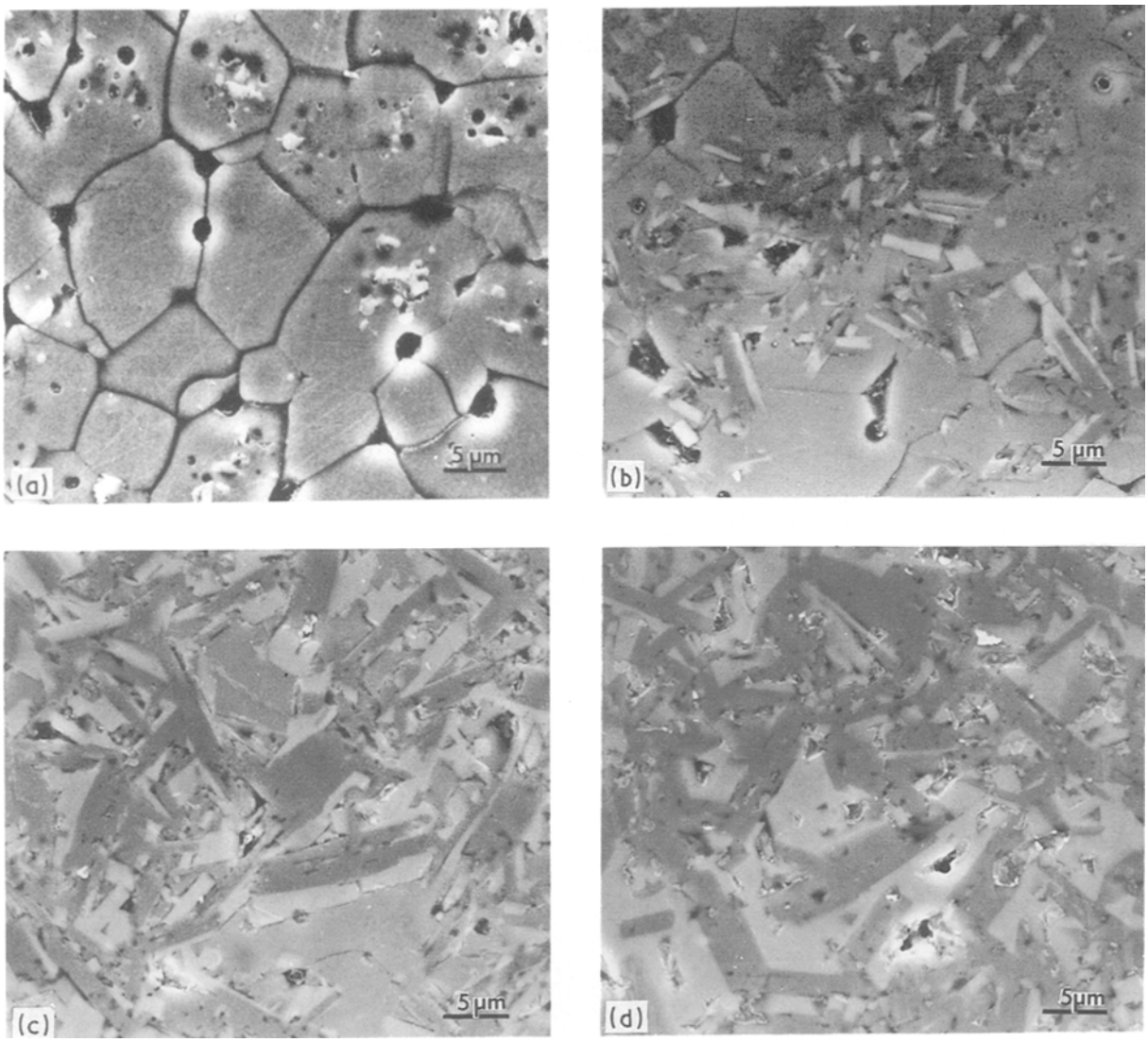

Figure 14 Micrographs of AT100 (1500° C) after annealing at 1150° C for: (1) 1.5 h, (b) 6 h, (c) 11 h, (d) 24 h.

contribution due to the microstructural change (needle-like Al_2TiO_5 grains) produced by MgO.

MgO reduces the coefficient of thermal expansion both in monophasic and composite samples.

In ZrO_2- and mullite-containing composites, MgO has proved to be very effective in stabilizing Al_2TiO_5 at 1150° C over 200 h. This finding indicates that a solid solution between Al_2TiO_5 and $MgTi_2O_5$ is also formed in the presence of 5 to 10 wt % $ZrSiO_4$.

Acknowledgements

One of the authors (H.W.) thanks the German Solvay Foundation and the Commission of the European Communities for the award of a fellowship. This work was supported by CICYT, Spain, project number MAT88-0156.

References

1. P. STINGL, J. HEINRICH and J. HUBER, in "Proceed-

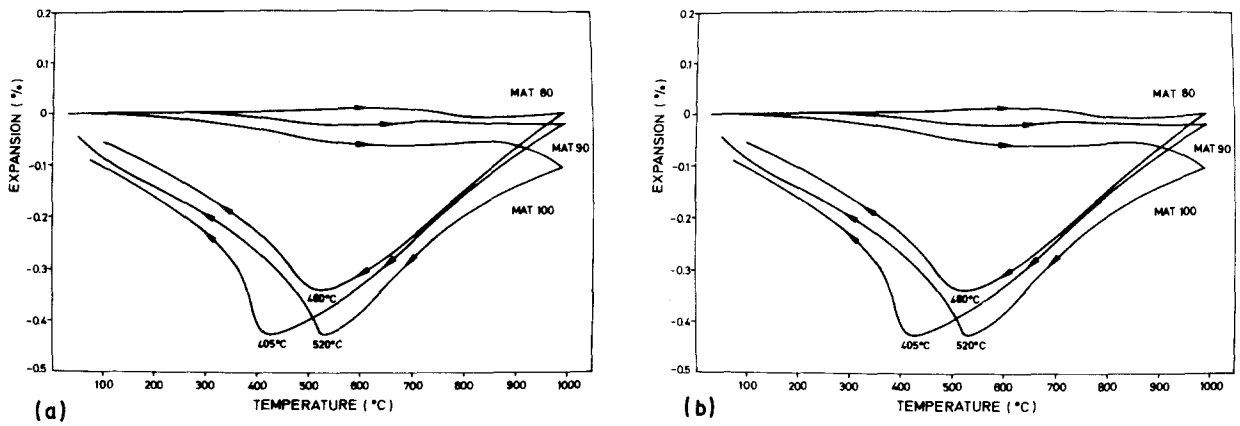

Figure 15 Thermal expansion curves between room temperature and 1000° C: (a) AT-series, (b) MAT-series. Heating rate 2° C min^{-1}, sintered at 1450° C, 2 h.

ings of the 2nd International Symposium on Ceramic Materials and Components for Engines", Lübeck-Travemünde, West Germany, April 1986, edited by W. Bunk and H. Hausner (DKG, Bad Honnef, 1986) p. 369.
2. H. HEINRICH, M. LANGER and J. E. SIEBELS, *ibid.*, p. 1155.
3. G. BAYER, *J. Less Common Metals* **24** (1966) 129.
4. J. J. CLEVELAND and R. C. BRADT, *J. Amer. Cer. Soc.* **61** (1978) 478.
5. P. PENA, S. de AZA and J. S. MOYA, in "Ceramic Microstructures '86. Role of Interfaces", edited by J. Pask and A. G. Evans (Plenum, New York, London, 1987) p. 847.
6. *Idem*, "Science of Ceramics", Vol. 14, edited by D. Taylor (Institute of Ceramics, Shelton, 1988) p. 751.
7. A. M. LEJUS, D. GOLDBERG and A. REVCOLEVSCHI, *Comt. Rend. Acad. Sci. Ser. C* **263** (1966) 1223.
8. A. S. BEREZHNOI and N. V. GUL'KO, *Ukrain. Khim. Zhur.* **21** (1955) 162.
9. P. PENA and S. de AZA, "Science of Ceramics", Vol. 12, edited by P. Vincenzini (Ceramurgica, Faenza, 1984) p. 201.
10. P. PENA, Ph D thesis, University Complutense of Madrid (1979).
11. P. PENA and S. de AZA, *Bol. Soc. Esp. Cerám. Vidr.* **15** (1975) 93.
12. M. SUGAI, R. NAITO, S. HIRANO and Sh. SOMIYA, *Yogyo Kyokai Shi* **79** (1971) 443.
13. E KATO, K. DAIMON and J. TAKAHASHI, *J. Amer. Ceram. Soc.* **63** (1980) 355.
14. Y. OHYA, M. HASEGAWA, Z. NAKAGAWA and K. HAMANO, Report of the Research Laboratory of Engineering Materials, Tokyo Institute of Technology, 12 November (1987) p. 81.
15. P. GMELIN, "Handbuch der Anorganischen Chemie", Vol. 41 (Springer, Berlin, 1977) p. 232.
16. H. WOHLFROMM, Th. EPICIER, G. THOMAS, P. PENA and J. S. MOYA, to be published.
17. J. de ANDRÉS, S. de AZA and J. S. MOYA, in "Proceedings of the 2nd International Symposium on Ceramic Materials and Components for Engines", Lübeck-Travemünde, West Germany, April 1986, edited by W. Bunk and H. Hausner (DKG, Bad Honnef, 1986) p. 299.
18. P. MIRANZO, P. PENA, J. S. MOYA and S. de AZE, *J. Mater. Sci.* **20** (1985) 2702.
19. Y. OHYA, K. HAMANO and Z. NAKAGAWA, *Yogyo Kyokai Shi* **94** (1986) 665.
20. J. J. CLEVELAND and R. C. BRADT, *J. Amer. Ceram. Soc.* **61** (1987) 478.
21. Y. OHYA, Z. NAKAGAWA and K. HAMANO, *ibid.* **70** (1987) C184.
22. N. CLAUSSEN, in "Advances in Ceramics", Vol. 12, "Science and Technology of Zirconia II", edited by N. Claussen, M. Rühle and A. H. Heuer (American Ceramic Society, Columbus, 1984).
23. Ch. HAHN, *Sprechsaal* **118** (1985) 1157.
24. K. HAMANO, Y. OHYA and Z. NAKAGAWA, *Int. J. High. Tech. Ceram.* **1** (1985) 129.
25. M. ISHITSUKA, T. SATO, T. ENDO and M. Y. SHIMAO, *J. Amer. Ceram. Soc.* **70** (1987) 69.

Received 18 April
and accepted 29 September 1989